ACS APPLIED MATERIALS & INTERFACES

www.acsami.org

Research Article

Sequentially Coated Wavy Nanowire Composite Transparent Electrode for Stretchable Solar Cells

Hyun Jeong Kwon,[▽] Geon-U Kim,[▽] Chulhee Lim, Jai Kyeong Kim, Sang-Soo Lee, Jinhan Cho, Hyung-Jun Koo, Bumjoon J. Kim,* Kookheon Char,* and Jeong Gon Son*

Cite This: *ACS Appl. Mater. Interfaces* 2023, 15, 13656−13667

Read Online

ACCESS | Metrics & More | Article Recommendations | Supporting Information

ABSTRACT: Recent advances in fabricating stretchable and transparent electrodes have led to various techniques for establishing next-generation form-factor optoelectronic devices. Wavy Ag nanowire networks with large curvature radii are promising platforms as stretchable and transparent electrodes due to their high electrical conductivity and stretchability even at very high transparency. However, there are disadvantages such as intrinsic nonregular conductivity, large surface roughness, and nanowire oxidation in air. Here, we introduce electrically synergistic but mechanically independent composite electrodes by sequentially introducing conducting polymers and ionic liquids into the wavy Ag nanowire network to maintain the superior performance of the stretchable transparent electrode while ensuring overall conductivity, lower roughness, and long-term stability. In particular, plenty of ionic liquids can be incorporated into the uniformly coated conducting polymer so that the elastic modulus can be significantly lowered and sliding can occur at the nanowire interface, thereby obtaining the high mechanical stretchability of the composite electrode. Finally, as a result of applying the composite film as the stretchable transparent electrode of stretchable organic solar cells, the organic solar cell exhibits a high power conversion efficiency of 11.3% and 89% compared to the initial efficiency even at 20% tensile strain, demonstrating excellent stretching stability.

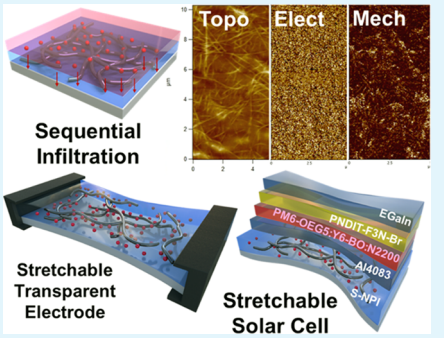

KEYWORDS: *stretchable transparent electrode, wavy Ag nanowire network, conducting polymer, ionic liquid, stretchable composite electrode*

INTRODUCTION

Recent developments in electronic devices[1] have focused on realizing innovative form factors that can be freely bent, rolled, folded, or further stretched to be expanded or reduced to a size desired by a user and conformably contacted or attached to soft substrates such as skin.[2−6] Among them, the optoelectronic field made the most remarkable progress with the release of previously unseen flexible electronic devices such as foldable mobile phones, rollable TVs, and seamless tile displays based on new form factors. Furthermore, as the next form factor, stretchable or deformable optoelectronic devices have been actively studied in recent years.[7−11] For stretchable and deformable optoelectronic devices, it is essential to secure the stretchability of the transparent electrode transmitting the lights and transporting the electrons. In the current flexible devices, flexible transparent electrodes are manufactured by thinly coating a rigid transparent electrode material such as indium tin oxide (ITO) on ultrathin glass or colorless polyimide flexible substrates.[12−14] However, since it is highly challenging to stretch a nonstretchable transparent electrode material structurally, a stretchable transparent electrode (STE) material needs to be newly developed.

The STEs have been very difficult to fabricate because they simultaneously should have high optical transparency, high electrical conductivity, and mechanical stability against various deformations (e.g., bending or stretching). Therefore, various approaches[15−17] have been tried to realize the STEs, including intrinsically stretchable materials, structural stretchability, and composite methods. In the intrinsic approach, graphene[18,19] and conducting polymers[20−22] are considered, but they do not have large deformability and have less conductivity under high transparency conditions. For structural stretchability, buckled or wavy shapes of flexible and conductive nanomaterials can be formed in a prestrained method onto elastomeric substrates.[23,24] However, carbon nanotubes (CNTs) and graphene still have relatively low conductivity,[25] and although Ag nanowire networks have high conductivity even at high transparency,[26−28] the nanowire strands are easily broken when deformed due to the brittleness of the nanowires.[29] Therefore, an approach for the STE that maintains a conductive penetration path even if a specific part is broken

Received: January 20, 2023
Accepted: February 20, 2023
Published: March 1, 2023

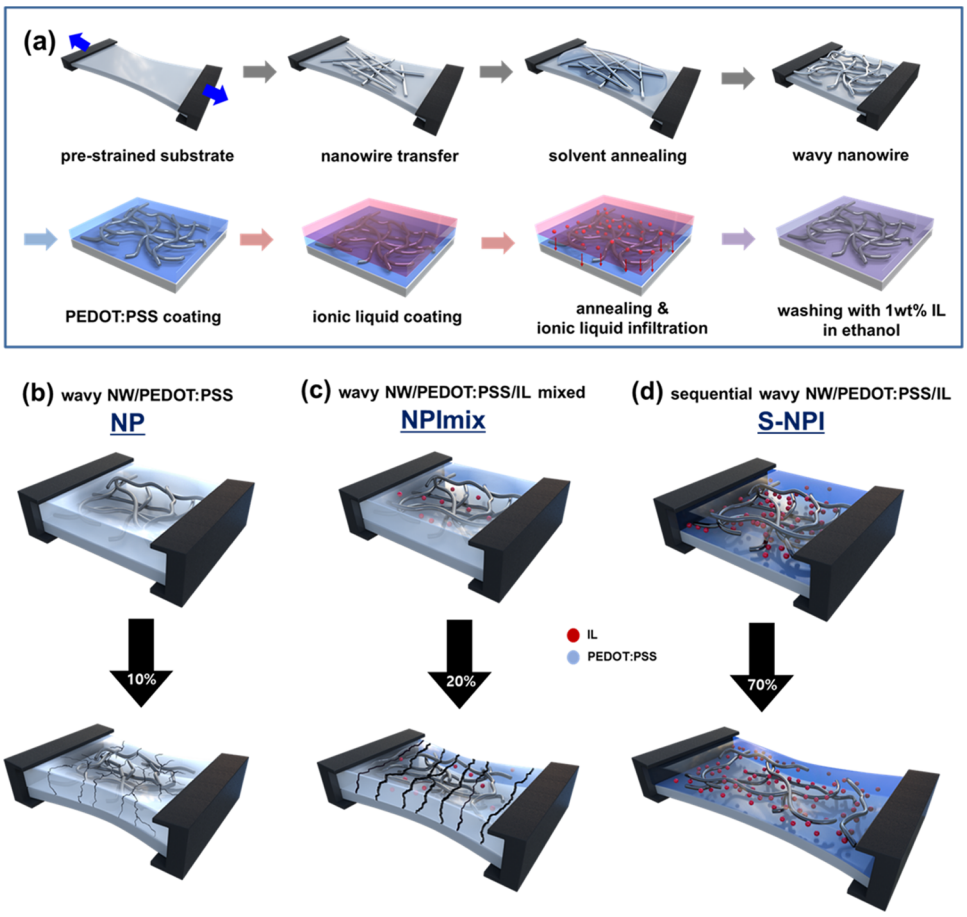

Figure 1. (a) Schematic illustration of the fabrication process of sequentially introduced wavy nanowire network/PEDOT:PSS/ionic liquid (S−NPI) composite electrode. (b−d) Schematic illustrations of (b) the pristine nanowire/PEDOT:PSS (NP) composite electrode resulting in cracks, (c) the nanowire/PEDOT:PSS/ionic liquid mixed (NPImix) composite electrode resulting in torn structure, and (d) the sequentially applied nanowire/PEDOT:PSS/ionic liquid (S−NPI) composite electrode showing highly stretchable behavior.

by applying a large number of nanowires at low transparency has been proposed.[30,31] Composite methods of Ag nanowires and graphene[5,32,33] or Ag nanowires and conducting polymers[31] have also been attempted, but the composite electrodes follow the limited stretchability of graphene or conducting polymers and frequently cause delamination at the interfaces. Conducting polymer and ionic liquid composites for mechanical stability under deformations and printability have been published, but the disadvantage of low conductivity at high transparency is still not overcome.[21]

Recently, by minimizing the influence of substrate and network junctions in the nanowire network, the problem that the prestrained nanowires firmly attached to the substrate form a short-term wrinkled structure causing concentrated stress in specific strand points resulting in their easy breakage could be solved.[34−37] At first, the nanowire network was floated on water like the Langmuir−Blodgett,[34−36] and then, compressive strain was applied to produce an in-plane wavy nanowire network with a large radius of curvature by compressing and sliding individual nanowire strands without the influence of the substrate. In addition, a solvent annealing process to the conventional prestrain method can weaken and slip the network junctions, leading to the structural rearrangement of wavy nanowires with large curvatures.[37] However, the wavy nanowire network-based STE with high transparency, high conductivity, and mechanical stability should still resolve the nonuniform areal conductivity and surface roughness due to the intrinsic structure properties and long-term stability due to the oxidation of silver nanowires. In particular, low surface uniformity in optoelectronic devices having an ultrathin film structure such as electroluminescence devices and organic photovoltaic cells inevitably resulted in that carriers are nonuniformly transported, recombination efficiency is significantly increased, and a short-circuit problem occurs severely.[38]

In this study, we focused on achieving additional full-coverage conductivity, low surface roughness, and long-term stability while maintaining the advantages of high transparency, high conductivity, and stretching stability of long-wavelength wavy nanowire networks as STEs. To this end, we introduced an intrinsically stretchable PEDOT:PSS/ionic liquid film into our wavy nanowire network. However, in general, simple nanowire network/PEDOT:PSS composite films enhance the mechanical modulus of the films like reinforced concrete with rebars embedded in it, which makes them less stretchable and more fragile. Therefore, to successfully fabricate composite-based STEs, in terms of conductivity, the synergy between the two conductive materials should occur, but mechanically, the interfacial properties between the nanowire and the conducting polymers are not good, so the conditions in which they slide each other should be created. However, simple PEDOT:PSS and ionic liquid mixtures easily preagglomerate in solution due to the strong interactions resulting in nonuniform coatings

https://doi.org/10.1021/acsami.3c00965
ACS Appl. Mater. Interfaces 2023, 15, 13656−13667

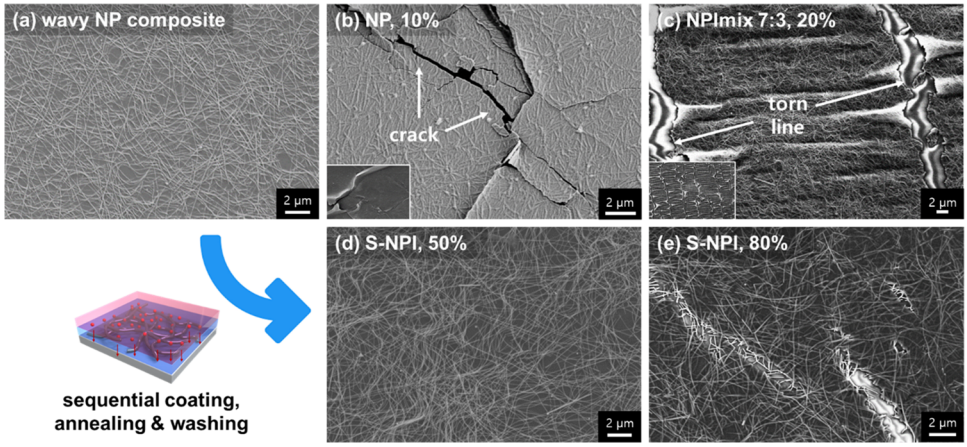

Figure 2. In situ scanning electron microscopy (SEM) images with a tensile stage of (a) the PEDOT:PSS-coated wavy nanowire network without any deformation, (b) the NP electrode under 10% strain, (c) the NPImix electrode under 20% strain, and (d and e) the S−NPI electrode under (d) 50% strain and (e) 80% strain, respectively.

with dirty marks. Therefore, we coated uniform and stable PEDOT:PSS films on the wavy nanowire network first and then sequentially coated an excess of ionic liquid and thermal annealing to allow plenty of ionic liquids to infiltrate into the composite film. This sequentially introduced wavy nanowire/PEDOT:PSS/ionic liquid (S−NPI) approach can effectively lower the interfacial adhesion between nanowires and polymers while maintaining the uniformity of the composite film. Through this method, we realized the STEs with full-coverage conductivity, a lower surface roughness (~5 nm of root-mean-square (RMS) roughness), and long-term stability (no resistance change for a month) while maintaining the highest levels of transparency (92.5%), high conductivity (33.5 Ω sq^{-1}), and mechanical stability under stretching (less than 2 of resistance change at 180% strain and after 1000 cycles of repetitive 50% stretching/releasing). Furthermore, by applying our STE for the fabrications of stretchable organic photovoltaic devices, which are highly sensitive to uniform conductivity and roughness, the high conversion efficiency of 11.3% and stability under 20% of tensile strain were successfully demonstrated, confirming its universal applicability.

RESULTS AND DISCUSSION

Figure 1a shows the scheme for the fabricating procedure of the stretchable transparent composite electrode. First, we formed the random nanowire network through vacuum filtration of Ag nanowire solution and transferred it to the uniaxially prestrained stretchable transparent substrates at 50%. After that, the prestrain was slowly released, while the Ag nanowire was annealed with water to form wavy nanowire networks of a large radius of curvature on the substrates. Here, we spin-coated the pristine PEDOT:PSS solution at 2000 rpm twice on the nanowire network to effectively fill in the gaps between the nanowires and flatten the transparent electrode uniformly. Afterward, an ionic liquid known to provide the flexibility of PEDOT:PSS, a rigid crystalline polymer, was introduced onto the nanowire/conductive polymer composite films by spin-coating. Then, through thermal annealing at 130 °C for 1 h, permeation of the ionic liquid into the composite film was induced, and the residual ionic liquid was removed through washing with 1 wt % ionic liquid containing ethanol to obtain a clean stretchable transparent composite electrode.

The characteristics of our stretchable transparent composite electrode were compared with a pristine nanowire/PEDOT:PSS (NP) composite electrode and a PEDOT:PSS/ionic liquid (mass ratio of 7:3) mixture coated on the nanowire (NPImix) composite electrode, as shown in Figure 1b−d. First, the morphologies of the NP composite films coated with PEDOT:PSS solutions on the wavy nanowire network are shown in Figure 2a. The thicknesses of polymer layers were controlled to ~80 nm. The wavy Ag nanowire network with a radius of curvature of approximately 3 μm is covered with PEDOT:PSS, but it can be easily observed in SEM due to its high conductivity. The NPImix composite films with a PEDOT:PSS/ionic liquid mixture also have similar morphologies.

Next, we investigated the morphological changes upon stretching the films through in situ tensile SEM experiments. The NP composite film dominantly showed a crack morphology with sharp edges even at 10% tensile strain, as shown in Figures 1b and 2b. When the conducting polymer is integrated into the wavy nanowire network, it fills the empty space of the nanowire network, increasing the modulus and brittleness like general composite materials. The matrix of the composite film holds the individual nanowires during stretching, thus inhibiting the deformation of the composite electrode. As a result, even at a strain of 10% or less, brittle fracture occurs without prior plastic deformation (no ductility), and the conductive paths are broken, making it impossible to operate as a stretchable electrode.

In PEDOT:PSS with additives, several studies have reported that using ionic plasticizers enhances conductivity and stretchability by weakening the strongly coupled electrostatic interaction between PEDOT and PSS and inducing swelling of PEDOT chains.[39,40] The composite film with a 7:3 mixture of PEDOT:PSS and 1-ethyl-3-methylimidazolium bis-(trifluoromethylsulfonyl)imide (EMIM:TFSI) ionic liquid shows relatively ductile properties as the PEDOT polymer swells in the ionic liquid. However, a high concentration of ionic liquid forms preaggregation with PEDOT:PSS in solution and induces nonuniform coating with dirty marks; thus, it is impossible to add a large amount of ionic liquid of 7:3 or more. The resulting NPImix composite film undergoes plastic deformation and ductile fracture at 20% strain in torn form, as shown in Figures 1c and 2c. The torn part was relatively

https://doi.org/10.1021/acsami.3c00965
ACS Appl. Mater. Interfaces 2023, 15, 13656−13667

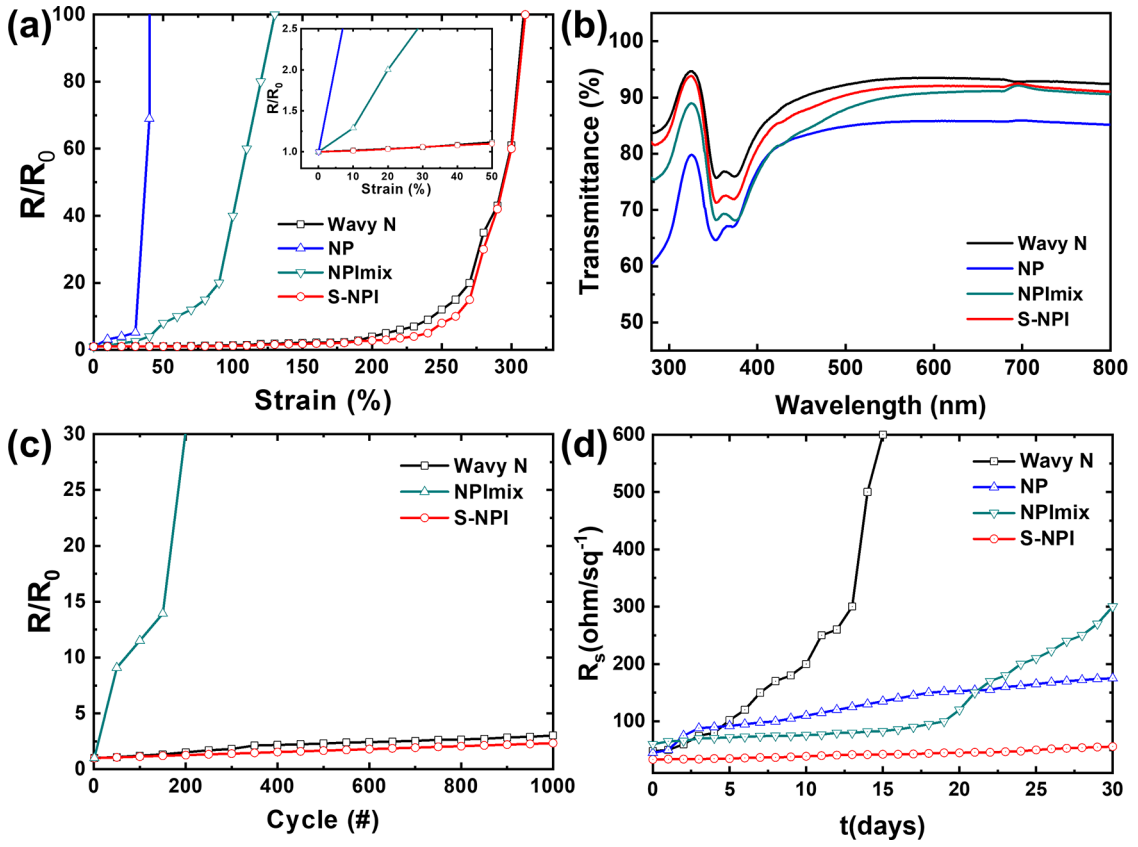

Figure 3. Performance comparison of (a) change in resistance according to uniaxial tensile strains, (b) ultraviolet−visible transmittance spectra, (c) change in resistance according to the repetitive 50% uniaxial stretching−releasing cycles, and (d) resistance change with time in air ambient air condition of STEs based on the pristine wavy N electrode, NP composite electrode, NPImix composite electrode, and S−NPI composite electrode.

clean and sharp, and no detachment of the nanowire from the matrix was observed, indicating that tensile stress was applied to the entire composite material. Through this phenomenon, it was found that mixing with the ionic liquid reduces the modulus of the composite film to some extent, but the amount of the ionic liquid had to be limited for the reliable and flat coating of the mixture.

Therefore, we attempted a sequential introduction method of the PEDOT:PSS matrix, which forms uniform composite films with the nanowire network, and excess ionic liquid infiltration, which provides sufficient ductility and induces sliding at the nanowire−matrix interface. The sequentially introduced wavy nanowire/PEDOT:PSS/ionic liquid (S−NPI) composite electrode did not form any tearing/fracture or structural changes at 50% tensile strain; only the morphologies in which the wavy nanowires in the prestrain direction were stretched straight in the tensile direction were observed in Figures 1d and 2d. From 80% strain, film fractures began to be observed, as shown in Figure 2e. In addition, in the fracture area, the polymer matrix was independently torn, and nanowire strands protruded between them and were connected to each other. The reason why the wavy nanowire strands are straightened without distortions of the network and the nanowires are seen separately at the torn edges is that the modulus of the polymer matrix and the interfacial adhesion between the polymer matrix and the nanowires are greatly lowered due to sufficient incorporation of the ionic liquid.

The sheet resistance of the transparent electrode and the change in resistance according to various tensile strains were observed with the transparency in the visible light region, as shown in Figure 3a,b. The pristine wavy nanowire (N) network electrode showed an initial sheet resistance of 39.7 Ω sq^{-1} and a transparency of 92% at 550 nm. In the strained states, the wavy nanowire-only network performed a very stable STE with resistance change ratios of less than 1.1 at 50% and less than 10 at various tensile strains up to 240%, as presented in our previous paper.[37] The NP composite film showed slightly improved sheet resistance of 38 Ω sq^{-1} due to the synergy of the two conductive materials, while the transparency was slightly lowered to 85% at 550 nm due to the inherent color of the PEDOT polymer. Under the strained states, the sheet resistance of the pure composite film increased dramatically over 70 times even at 40% strain compared to the initial resistance, which was consistent with the SEM result of brittlely cracked composite film at 10% strain in Figure 2b. The NPImix electrode increased the sheet resistance to 62 Ω sq^{-1} and decreased the transparency to 89%. The reason is that the PSS of PEDOT:PSS and the cations of the ionic liquid create insoluble gels to form their own domains and disrupt the electrical conduction pathway between PEDOT and the nanowires. In addition, small-sized agglomerations and resulting marks of PEDOT/ionic liquid were still formed even at low concentrations, making it difficult to obtain uniform and highly transparent films. When the tension was applied to the NPImix composite film, it was found that the resistance increased significantly even at low strain, such as more than 8 times increase in resistance at 50% strain. This result is consistent with the primarily torn SEM image at 20% strain in Figure 2c.

https://doi.org/10.1021/acsami.3c00965
ACS Appl. Mater. Interfaces 2023, 15, 13656−13667

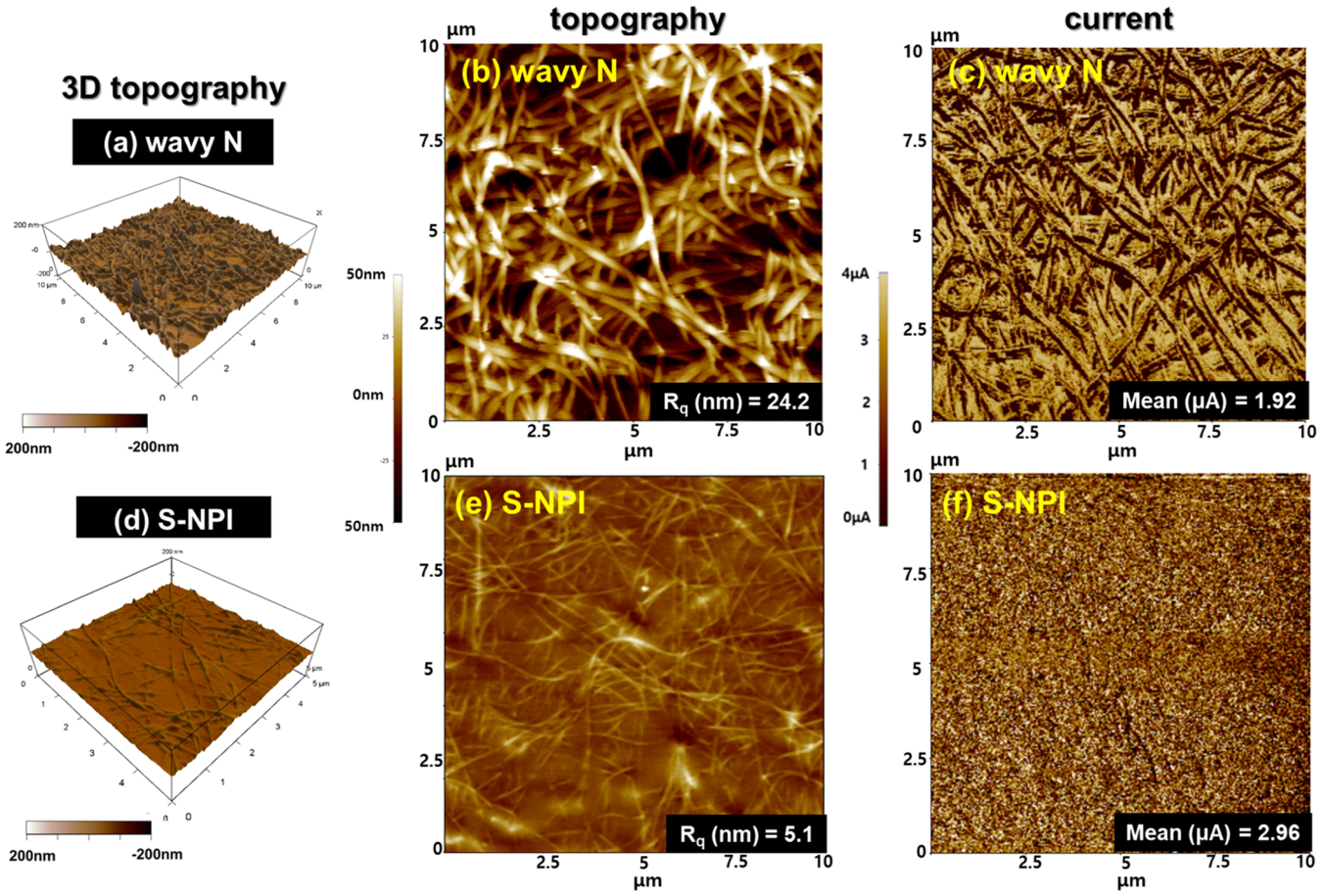

Figure 4. (a, b) AFM topographical images and (c) their current image of conductive AFM of the pristine wavy N electrode. (d, e) AFM topographical images and (f) their current image of the S−NPI composite electrode.

On the other hand, our S−NPI composite film showed high transparency (92.5% at 550 nm) almost corresponding to the transparency of the pristine wavy nanowire network, and the initial sheet resistance was improved to 33.5 Ω sq^{-1}. In the PEDOT polymer, whose colorfulness changes greatly depending on the doping level, the ionic liquid acts as a dopant for the PEDOT to greatly increase the doping level, increasing the conductivity and making the color fainter.[41] Also, by forming a relatively flat film, diffuse reflection from surface irregularities can be lowered. For the conductivity, in addition to the doping effect, the PSS-based nonconductive gel formed with the ionic liquid could be removed through the washing process, thus maintaining high conductivity uniformly. With the stretching, the sheet resistance changes were 1.08 even in the tensile state of 80%, showing very stable electrical conductivity similar to the pristine wavy nanowire network without polymers. For higher strain, the change in resistance finally reached a value of 2.8 times at 200% strain, and the films withstood mechanical strains up to 330% tensile strain. When a cycle test of repeatedly applying and releasing to 50% strain was performed (Figure 3c), the resistance change ratio was still less than 2 for up to 1000 cycles, indicating even higher mechanical stability than the pristine nanowire network, whereas the NPImix film was already unable to perform the STE role at 200 cycles or less.

Long-term stability, which was pointed out as a weakness of silver nanowire-based electrodes due to oxidation, was also investigated and is shown in Figure 3d. Under ambient conditions, a resistance change of more than 20 times was observed in the pristine N electrode within 15 days, whereas in the case of the polymer layer-coated electrodes, the resistance change was relatively well maintained over 1 month. However, in the case of NPImix, since the ionic liquid and PEDOT:PSS already meet in solution to form an insoluble gel containing a large amount of hygroscopic PSS, the polymer film acts as a barrier to some extent but shows a rapid change in resistance after 20 days, resulting in low long-term stability. Especially our S−NPI composite electrode showed almost no changes in resistance even after 30 days. This is because a large amount of hydrophobic ionic liquid fills the free volume between the polymer chains to passivate from oxidation. In addition, the hygroscopic PSS polymers are also considerably removed through the washing process. Based on this result, our composite electrode newly achieved long-term stability while maintaining the high transparency, electrical conductivity, and mechanical stability of the previous pristine nanowire-based STEs.

To investigate the topographical morphologies and overall conductivity of our composite electrode compared with the pristine N electrode, we executed conductive atomic force microscopy (c-AFM) analysis, as shown in Figure 4. The nanowire network with a diameter of 25 nm (topographical images in Figure 4a,b) was measured that a height difference between the nanowire-junction area and blank substrate was more than 50 nm and the root-mean-square roughness (R_q) of the surface was approximately 24 nm. In contrast, AFM

https://doi.org/10.1021/acsami.3c00965
ACS Appl. Mater. Interfaces 2023, 15, 13656−13667

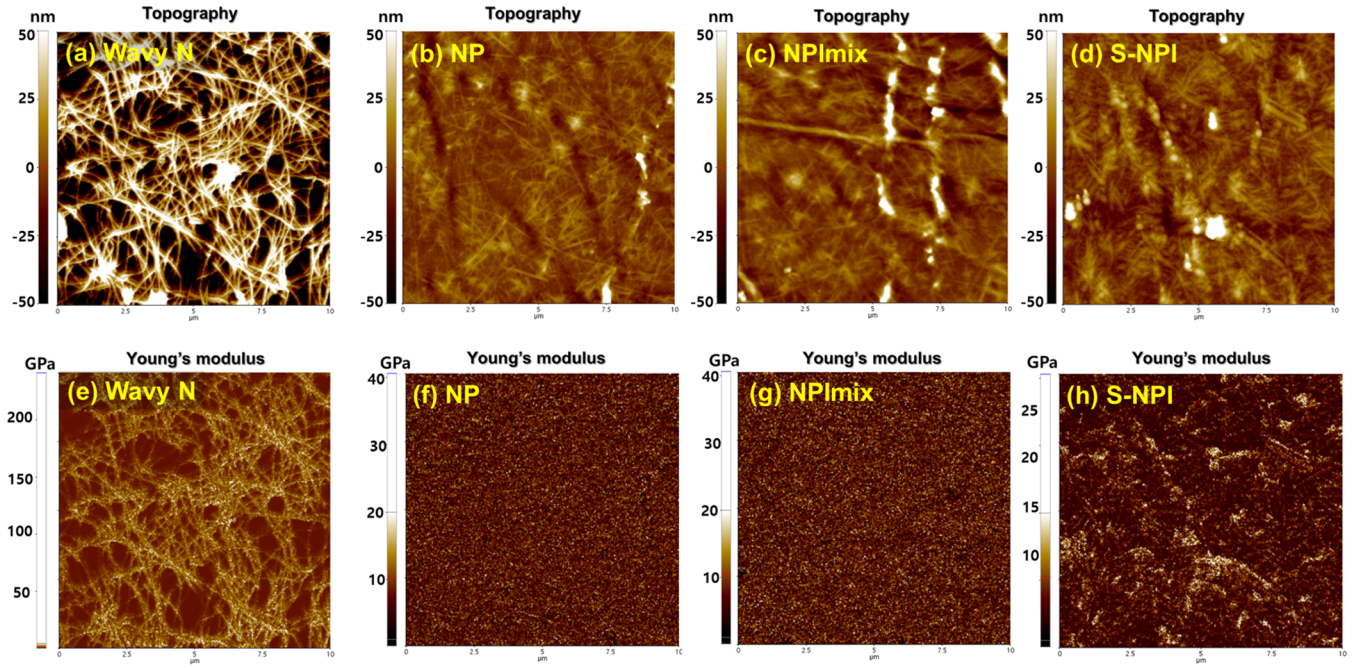

Figure 5. (a–d) Topographical images and (e–h) elastic modulus mapping images from the AFM PinPoint nanomechanical mode of (a, e) the pristine wavy N electrode, (b, f) NP electrode, (c, g) NPImix composite electrode, and (d, h) S–NPI composite electrode. Images are all 10 × 10 μm^2.

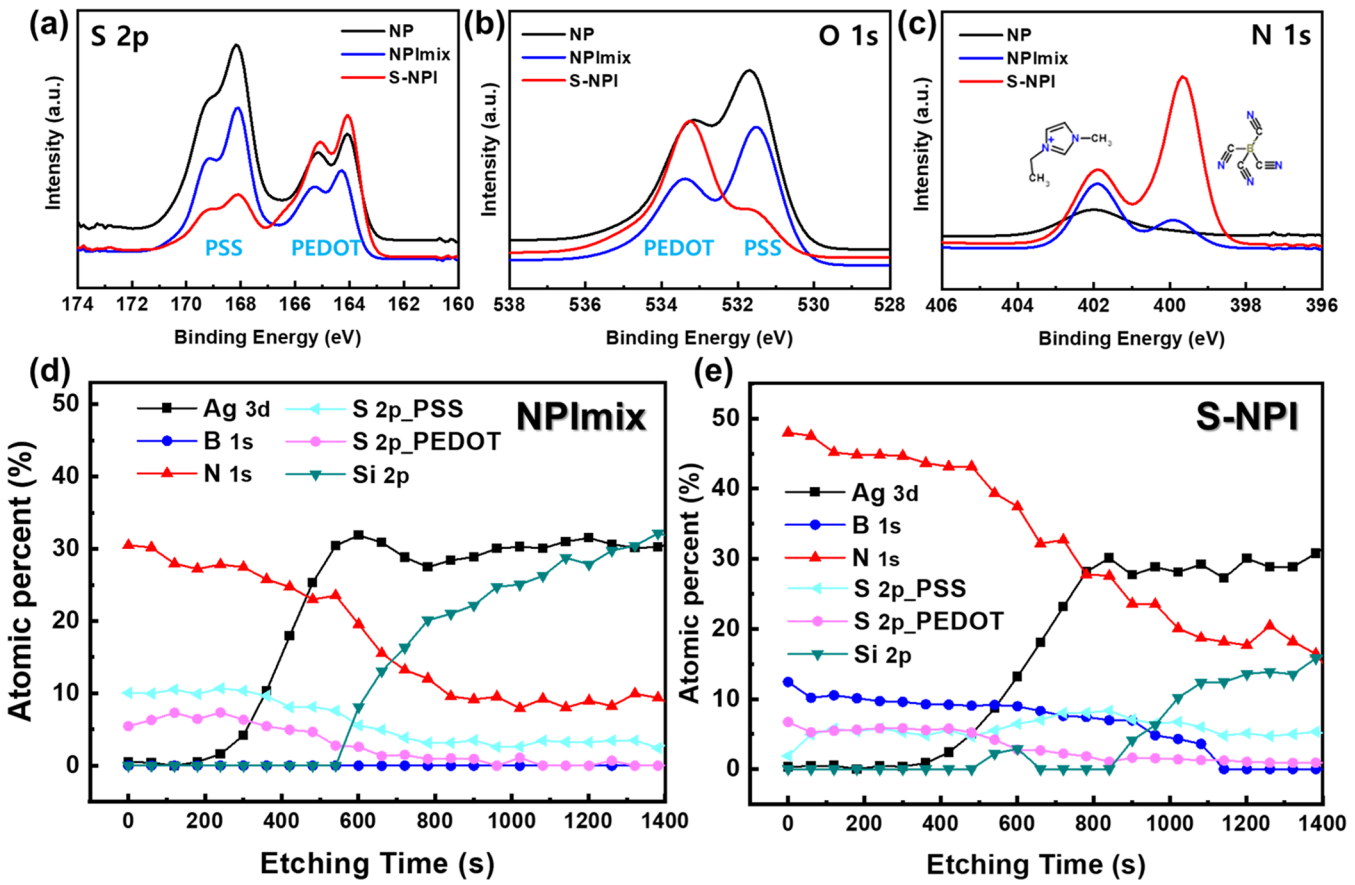

Figure 6. (a) S 2p, (b) O 1s, (c) N 1s XPS spectra of the NP, NPImix, and S–NPI composite electrodes. (d, e) Relative atomic composition of the etching time at various depths of the (d) NPImix and (e) S–NPI composite electrodes.

topographical images in Figure 4d,e showed that the S–NPI electrode was filled with conductive PEDOT/ionic liquid at the blank space and the nanowires were primarily embedded in the polymer film so that the topographical height of the

https://doi.org/10.1021/acsami.3c00965
ACS Appl. Mater. Interfaces 2023, 15, 13656–13667

nanowires was not high compared to the pristine nanowire network, resulting in a low RMS roughness of 5.1 nm. In the c-AFM image of the N electrode in Figure 4c, the texture of the nanowires was clearly observed and the intensity difference from the blank area was clearly visible. The average current at the N electrode surface was measured to be 1.92 μA. In contrast, the current AFM image of the S−NPI electrode in Figure 4f showed a flat morphology, so the existence of nanowires was hardly recognized, and the average current was observed as 2.96 μA, which is significantly higher than the value for the N electrode in Figure 4c. This uniform current indicates that our composite electrode exhibits very uniform conduction properties across the entire surface regardless of the presence of nanowires. Thus, the AFM study revealed that the nanowires are well embedded in the conductive polymer, enabling low surface roughness and uniformly distributed conductivity.

To investigate the mechanical property distributions of the composite electrodes at the nanoscale,[42,43] we analyzed Young's modulus of the microscopic area through mapping with the PinPoint Nanomechanical mode,[42] as shown in Figure 5. The height (Figure 5a) and modulus (Figure 5e) images of the N electrode similarly revealed clear nanowire textures, and the nanowire area showed a modulus of 10 to 200 GPa, while the vacant area showed a value similar to the PDMS's modulus value of 1−3 MPa. On the other hand, the height images of all of the polymer-coated nanowire composite network films (Figure 5b−d) similarly showed most embedded nanowires with much less surface roughness. Here, the modulus mapping images of the NP and NPImix composite films in Figure 5f,g showed only monotonic planar morphology with mean modulus values of 8.6 and 7.4 GPa and no nanowire traces. These flat modulus morphologies mean that the first two composites mechanically act as a one-piece, like reinforced concrete with rebars. However, the modulus mapping image of the S−NPI composites in Figure 5h showed faint but clear nanowire morphology, and the average modulus was significantly lower at 2.7 GPa compared to other composite films. This inhomogeneous modulus map indicates that nanowire fillers and the polymer/ionic liquid matrix can move independently in composite films under deformations, like rebars in sand. This mechanically independent filler and matrix system can maintain its own structural stretchability and provide relatively higher mechanical stability at larger strains.

X-ray photoelectron spectroscopy (XPS) analysis was performed on the composite STE films, as shown in Figure 6 to analyze the difference in the chemical composition of the films. Here, since the XPS peaks of the $TFSI^-$ anion in the ionic liquid and PEDOT:PSS overlap, the composite electrodes were prepared differently using another hydrophobic ionic liquid anion, tetracyanoborate anion (TCB^-).[40,44,45] The S−NPI electrode with the EMIM:TCB also showed superior mechanical stability under tensile strains, as shown in Figure S1. In the S 2p spectrum of the S−NPI composite STEs (Figure 6a), the PEDOT peak at 163.8−165 eV was higher and the PSS peak at 168.9−170 eV was lower than those of the NP and the NPImix composite film. This result indicates that the excess ionic liquid ($EMIM^+$ and TCB^-) separates electrostatically bound PEDOT and PSS, followed by the removal of the well-dispersible PSS during the washing process. In the NPImix composite films, PEDOT and PSS can also be separated, but the PSS still exists in the film. This result explains why the S−NPI composite films have better conductivity. Even in the O 1s (Figure 6b) spectra, the 533.2 eV region peak (PSS) of the S−NPI composite STE is much smaller than those of other STEs, consistent with the above results.

In addition, in the N 1s spectra contained in the ionic liquid (Figure 6c), the 398.2 eV peak of $EMIM^+$ was observed with similar intensity in both the NPImix STE and the S−NPI STE, but a peak at 400.5 eV representing the TCB^- ion was significantly observed only in the S−NPI composite STE. The spectrum of B 1s only in the TCB^- ion in Figure S2a also showed a fairly strong peak only in the S−NPI composite STE. In the NPImix composite, strongly aggregated $EMIM^+$ and PSS^- polymer chains could remain somewhat on the film during spin-coating, but relatively few TCB^- ions, which were well dispersed in the solvent, remained. We balanced the cation/anion of the ionic liquid in the composite film by sequentially introducing an excess of the ionic liquid and adding a small amount of the ionic liquid even during the washing process. The presence of this large amount of intact ionic liquid is thought to effectively reduce the modulus of the matrix and result in independent deformation behavior between the filler and matrix. In addition, as a result of XPS depth profiling using Ar ion beam, the nitrogen and boron fractions representing the amount of ionic liquid and TCB^- ions, respectively, were consistently higher throughout the thin film in the S−NPI composite STE than in the NPImix STE. The PEDOT fraction relative to the PSS fraction was also observed to be high throughout the film. These depth profiles indicate that the ionic liquid can sufficiently penetrate the bottom surface of the film during the annealing process and that a higher amount of intact ionic liquid can be contained and the PSS can be removed throughout the S−NPI composite film.

Additionally, the composite-based stretchable transparent electrode can adjust electronic properties such as a work function[46] affecting the hole injection barrier of an optoelectronic device using various ionic liquids. The intrinsic work function values of materials of our STE are 4.2−4.3 eV for the silver nanowires and 4.8 eV for the PEDOT:PSS, lower than those of commercial ITO glass electrodes (4.7−5.1 eV). After sequentially introducing each of EMIM:TCB, EMIM:TFSI, and 1-butyl-1-methylpyrrolidinium bis(trifluoromethanesulfonyl) imide (Bmpyr:TFSI) as ionic liquids in sequential composite films, the ultraviolet photoelectron spectroscopy (UPS) measurements were executed (Figure S3). When only the PEDOT:PSS was coated on the wavy NW, the work function value of 4.97 eV was much higher than that of the pristine wavy NW (3.97 eV). The ionic liquid-containing composite electrodes have various work functions, such as 4.85 eV for EMIM:TCB, 5.11 eV for EMIM:TFSI, and 5.09 eV for Bmpyr:TFSI. In particular, the TFSI anion-containing films achieved a high work function of 5.11 eV, and it is considered that the work function can be adjusted according to the type of anions doped in the PEDOT polymer.

Stretchable organic solar cells (SOSCs)[38,47,48] are attracting considerable attention as an off-grid power source for next-generation skin-attachable devices.[49−56] However, it is very difficult to apply the conventional SCEs to the OSC, which is very sensitive to the conductivity uniformity and surface roughness of transparent electrodes. In addition, it is also challenging to make all components of the OSC intrinsically stretchable, thus intrinsically stretchable organic solar cells with a high power conversion efficiency (PCE) of over 10% have

https://doi.org/10.1021/acsami.3c00965
ACS Appl. Mater. Interfaces 2023, 15, 13656−13667

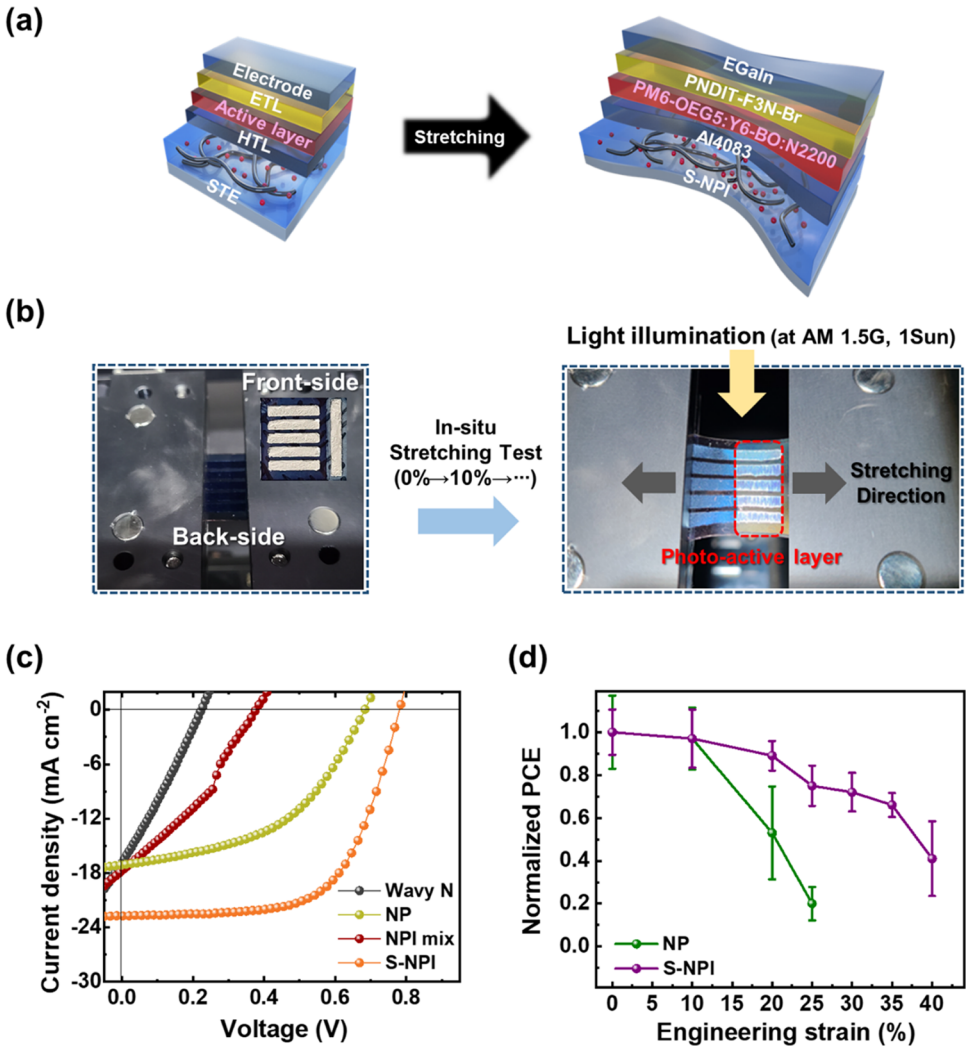

Figure 7. (a) Schematic illustration of the device structure of a stretchable organic solar cell (SOSC). (b) Photographic images of our SOSCs and in situ stretching test. (c) Current density−voltage (J−V) curves of each SOSC with different STEs prior to applying external tensile strain. (d) Normalized PCEs as a function of the applied strain of NP- and S−NPI-based SOSCs.

Table 1. Photovoltaic Performances of SOSCs Depending on the Type of STEs

system	V_{oc} (V)	J_{sc} (mA cm^{-2})	FF	PCE$_{max\ (avg)}$ (%)
wavy N	0.222 (0.206 ± 0.017)	16.83 (15.02 ± 1.78)	0.27 (0.27 ± 0.01)	1.03 (0.84 ± 0.19)
NP	0.697 (0.674 ± 0.015)	17.11 (16.37 ± 0.75)	0.48 (0.45 ± 0.05)	5.59 (4.97 ± 0.85)
NPImix	0.377 (0.239 ± 0.194)	17.72 (17.47 ± 0.36)	0.34 (0.29 ± 0.06)	2.24 (1.34 ± 1.27)
S−NPI	0.781 (0.773 ± 0.013)	22.74 (22.33 ± 0.86)	0.63 (0.59 ± 0.04)	11.26 (10.16 ± 1.08)

only recently been reported.[38,49,57,58] To explore the potential of the S−NPI composite STEs, we fabricated the SOSCs with a device configuration of thermoplastic polyurethane (TPU) elastomer (substrate)/S−NPI STE (bottom electrode)/AI4083 (hole transport layer, HTL)/photoactive layer/PNDIT-F3N-Br (electron transport layer, ETL)/eutectic gallium−indium (EGaIn) (top electrode) (Figure 7a).[59] For the solvent orthogonality of the SOSC process, the substrate was changed from PDMS to TPU. First, the N, NP, NPImix, and S−NPI STE was fabricated on a stretchable TPU substrate (a thickness of ∼100 μm). Then, the PEDOT:PSS-based AI4083 as a HTL was spin-coated for a thickness of ∼30 nm onto each STE, followed by mechanically durable PM6-OEG5:Y6-BO:N2200 ternary blend as an active layer was deposited for a thickness of ∼100 nm.[47,48] As an ETL, polymeric PNDIT-F3N-Br (∼5 nm) was selected for improved elasticity.[60] Finally, to facilitate the Ohmic contact between the top electrode and the organic layer without uneven stresses even under tensioned states, liquid metallic EGaIn was air spray-coated using a pattern mask to form the stretchable top electrode.[59,61] The actual images of SOSC and *in situ* stretching tester and the resulting SOSC performances depending on the applied strains are displayed in Figure 7b and Table 1, respectively.

Among the four STEs, the SOSC with the S−NPI composite STE achieved the highest PCE of 11.3% with the photovoltaic parameters of open−circuit voltage (V_{oc}) = 0.78 V, short-circuit current (J_{sc}) = 22.74 mA cm^{-2}, and fill factor (FF) = 0.63), mainly owing to the lowest surface roughness of 5.1 nm and sheet resistance of 33.5 Ω sq^{-1} of the S−NPI composite

https://doi.org/10.1021/acsami.3c00965
ACS Appl. Mater. Interfaces 2023, 15, 13656−13667

Table 2. Photovoltaic Performances of SOSCs Depending on the Applied Strains

system	strain (%)	V_{oc} (V)	J_{sc} (mA cm^{-2})	FF	PCE$_{max\ (avg)}$ (%)	normalized PCE$_{avg}$
NP	0	0.697 (0.674 ± 0.015)	17.11 (16.37 ± 0.75)	0.48 (0.45 ± 0.05)	5.59 (4.97 ± 0.85)	1.00
	10	0.712 (0.683 ± 0.025)	15.90 (15.31 ± 0.51)	0.47 (0.46 ± 0.04)	5.30 (4.82 ± 0.72)	0.97
	20	0.652 (0.514 ± 0.183)	14.66 (14.21 ± 1.88)	0.40 (0.33 ± 0.07)	3.78 (2.61 ± 1.08)	0.53
	25	0.524 (0.397 ± 0.163)	7.31 (7.01 ± 0.28)	0.34 (0.35 ± 0.07)	1.30 (0.98 ± 0.39)	0.20
S−NPI	0	0.781 (0.773 ± 0.013)	22.74 (22.33 ± 0.86)	0.63 (0.59 ± 0.04)	11.26 (10.16 ± 1.08)	1.00
	10	0.779 (0.779 ± 0.001)	22.46 (22.06 ± 0.96)	0.64 (0.57 ± 0.07)	11.12 (9.83 ± 1.38)	0.97
	20	0.768 (0.759 ± 0.012)	21.07 (20.84 ± 0.79)	0.60 (0.57 ± 0.04)	9.73 (9.04 ± 0.70)	0.89
	25	0.766 (0.750 ± 0.022)	20.57 (20.27 ± 1.40)	0.56 (0.50 ± 0.06)	8.76 (7.64 ± 0.95)	0.75
	30	0.753 (0.713 ± 0.033)	19.73 (19.90 ± 0.80)	0.54 (0.52 ± 0.03)	7.99 (7.35 ± 0.91)	0.72
	35	0.649 (0.688 ± 0.048)	19.45 (18.54 ± 1.10)	0.56 (0.52 ± 0.05)	7.12 (6.67 ± 0.57)	0.66
	40	0.644 (0.560 ± 0.151)	17.26 (16.39 ± 0.99)	0.47 (0.43 ± 0.09)	5.20 (4.15 ± 1.77)	0.41

STE. This result represents one of the best performances among the reported Ag NW-based SOSCs to date (Table S1). In contrast, the N, NP, and NPImix-based SOSCs showed relatively low PCEs of 1.0, 5.6, and 2.2%, respectively. In particular, each device exhibited nonideal V_{oc}s and low FFs (V_{oc} = 0.22 V and FF = 0.27 for the N electrode, V_{oc} = 0.70 V and FF = 0.48 for the NP electrode, and V_{oc} = 0.38 V and FF = 0.34 for the NPImix electrode), which might be a result of the nonuniform contact between the STE and the photoactive layer that hampers efficient charge transport and collection in the device.

Next, we evaluated the stretchability of NP and S−NPI composite STE-based SOSCs (Figure 7c and Table 2). The SOSC based on the S−NPI composite STE maintains over 89% (PCE$_{avg}$ of 9.0%) compared to the initial PCE even at 20% of tensile strain, demonstrating excellent stretchability. In contrast, the PCE$_{avg}$ of NP STE-based SOSC was dropped to 2.6 at 20% strain. This superior photovoltaic performance under deformations proved that our sequential composite SCE could be stably stretched while ensuring high transparency, uniform and high conductivity, and low roughness. Overall, the S−NPI composite-based STE shows great potential to simultaneously achieve a high performance and stretch stability of optoelectronic devices such as SOSCs, which are very sensitive to surface roughness and uniform conductivity.

CONCLUSIONS

In summary, we fabricated a stretchable and transparent composite electrode composed of a sequentially introduced wavy Ag nanowire network, PEDOT:PSS conducting polymer, and ionic liquid to ensure overall conductivity, low roughness, and long-term stability while maintaining the excellent performance of the stretchable transparent electrode. In particular, to prevent the intrinsic increase in brittleness of the polymer nanocomposites, ionic liquids are introduced to soften the polymer and lower the interfacial stability between the components, allowing them to slide during tension. In addition, while simply mixed intimately interacting PEDOT:PSS and ionic liquid quickly form agglomerates making subsequent processing difficult, sequential introduction allows much greater amounts of ionic liquid to be embedded within the composite film without disturbing uniformity, maximizing stretchability. Furthermore, the long-term stability of the nanowire-based electrode was increased by removing the hydrophilic PSS and filling the free volume of the polymers. Since various ionic liquids can be used, the work function of the electrode can be adjusted and the performance of the stretchable optoelectronic device can be optimized. By applying our composite film as a stretchable transparent electrode for a stretchable organic solar cell, a high conversion efficiency of 11.3% and 89% of efficiency retention even under a tensile strain of 20% was obtained. Through this, we presented a reliable approach to how a silver nanowire-based stretchable transparent electrode with high transparency, high conductivity, and stretch stability can be applied as a stretchable optoelectronic device. We believe that this approach will play an essential role in greatly increasing the freedom of form factor and significantly expanding new markets of stretchable optoelectronic devices.

EXPERIMENTAL SECTION

Materials. Ag NW dispersion in ethanol (0.5 mg mL^{-1}) was purchased from SG Flexio Co. Ltd., with an average diameter of 27 nm and a length of 22 μm. A commercial poly(tetrafluoroethylene) (PTFE) membrane having 0.2 μm pores was obtained from Millipore (JGWP04700). Poly(dimethylsiloxane) (PDMS, Sylgard 184, Dow Corning Ltd.) substrates were prepared by mixing the prepolymer and curing agent in a 10:1 weight ratio, then poured on the glass substrate, and cured at 80 °C for 3 h. Transparent thermoplastic polyurethane (TPU) substrates with 0.1 mm thickness were purchased from Ventwin Ltd. PEDOT:PSS aqueous solution (Clevios PH1000) was purchased from Clevios. 1-Ethyl-3-methylimidazolium bis-(trifluoromethylsulfonyl)imide (EMIM:TFSI; 98%) was prepared by Tokyo Chemical Industry, and 1-ethyl-3-methylimidazolium tetracyanoborate (EMIM:TCB; 99.5%) was purchased from Sigma-Aldrich. Bmpyr:TFSI was purchased from Kanto Chemical Co. Inc. The PM6-OEG polymer donor with a weight-average molecular weight of 358 kg mol^{-1} and dispersity of 3.2 was prepared with the same synthetic route reported in our previous work.[47] The N2200 with a weight-average molecular weight of 408 kg mol^{-1} and dispersity of 2.6 was prepared by the Stille coupling reaction following the previous literature method. The small molecular acceptor, Y6-BO, was purchased from *Derthon*. Poly[(9,9-bis(3′-((*N*,*N*-dimethyl)-*N*-ethylammonium)propyl)-2,7-fluorene)-*alt*-5,5′-bis(2,2′-thiophene)-2,6-naphthalene-1,4,5,8-tetracaboxylic-*N*,*N*′-di(2-ethylhexyl)imide]-dibromide (PNDIT-F3N-Br) was synthesized according to the reported method.[60] PEDOT:PSS (AI4083) was purchased from *Heraeus*. Indium (In, 99.99% purity) and gallium (Ga, 99.99% purity) were obtained from TASCO. EGaIn was formed by mixing 24.5 wt % In and 75.5 wt % Ga. Then, the EGaIn mixture was heated at 150 °C for 1 h.

Prestrain Process with Solvent Annealing of the Ag NW Network. First, 10 cm × 10 cm of PDMS substrate with an average thickness of 200 μm was stretched up to 50% using tension equipment. The Ag NW solution dispersed in ethanol was filtered using vacuum filtration with a PTFE membrane and transferred onto the prestrained PDMS substrate. After that, the solvent annealing was executed by dropping distilled water onto the entire network area and waiting for 10 min; then, the applied strain was slowly released with

https://doi.org/10.1021/acsami.3c00965
ACS Appl. Mater. Interfaces 2023, 15, 13656−13667

0.001 mm s^{-1}. After the stain releasing, the distilled water was quickly removed with nitrogen blowing.

Preparation of the Stretchable Transparent Composite Electrode. First, we spin-coated the pristine PH1000 PEDOT:PSS solution on the Wavy Ag NW network at 2000 rpm and then annealed it at 60 °C for 1 h for the pristine NP composite film. For the NPImix composite, PEDOT:PSS and the ionic liquid were mixed with a content weight ratio of 7:3, and the mixed solution was spin-coated on the wavy NW network at 2000 rpm and dried at 60 °C for 1 h. For the S−NPI composite film, the PEDOT:PSS solution was spin-coated twice (for compensating washed polymers) at 2000 rpm onto the wavy NW network, followed by spin-coating nondiluted ionic liquids at 2000 rpm and annealed at 60 °C for 1 h. Excess ionic liquid with soluble polymer chains was removed by washing with 1 wt % ionic liquid containing ethanol.

Preparation of the Stretchable Solar Cell. Normal-type SOSCs with a device configuration of TPU substrate/S−NPI or other STEs/AI4083/photoactive layer/PNDIT-F3N-Br/eutectic gallium−indium (EGaIn) (top electrode) were fabricated. AI4083 (with FS-30 0.5 vol %) HTL was spin-coated at 2500 rpm for 40 s on the STE-deposited TPU substrate and dried to 100 °C for 20 min. Subsequently, the active layer solution (PM6-OEG5/Y6-BO/N2200 = 1:1:0.2) was dissolved together in chlorobenzene (CB) with an optimized condition (total concentration = 18 mg mL^{-1}, and 1-chloronaphtalene (CN) 0.5 vol %) and then heated for 2 h on a 90 °C plate. Next, the solution was spin-cast onto the AI4083 HTL at 2000 rpm and 30 s. Then, as an ETL, a PNDIT-F3N-Br of 1 mg mL^{-1} in methanol was spun at 2500 rpm for 40 s. Finally, EGaIn liquid metal was sprayed on the ETL through a deposition mask.

Stretchable Solar Cell Measurement. The weight-average molecular weight (M_w) and dispersity ($Đ$) of the polymer donor (PM6-OEG5) and acceptor (N2200) were determined by gel permeation chromatography (GPC) analysis with an Agilent GPC 1200 instrument equipped with a refractive index detector, in the condition of *ortho*-dichlorobenzene (*o*-DCB) eluent at 80 °C with polystyrene standards. A Keithley 2400 SMU instrument was used to measure the all-PSC efficiency under an air mass 1.5 G solar simulator (100 mW cm^{-2}, solar simulator: K201 LAB55, McScience), satisfying the Class AAA, ASTM Standards. The K801SK302 of McScience was used as a standard silicon reference cell to calibrate the exact solar intensity. The*in situ* stretching machine for measuring the efficiency of SOSCs was built with a solar simulator (K3100 IQX, McScience Inc.). We used a shadow mask with a fixed area (0.06 cm^{-2}) to measure the solar cell efficiency in stretched conditions.

Characterization Methods. The conductivity of electrodes was measured using a four-point probe (Cresbox, Napson). The transmittance spectra of wavelengths from 400 nm to 900 nm were collected using a ultraviolet−visible−near-infrared (UV−vis-NIR) spectrometer (V-600, Jasco). The morphology of composites was examined with a field emission scanning electron microscope (FE-SEM, Sigma 300, Zeiss) with an in situ stretching stage (Microtest 2kN tensile stage, Deben U.K. Ltd.) at 1−3 kV electron acceleration voltage. The stretching test was performed using a motorized linear stage connected to a source meter (Keithley 2400, Tektronix) and equipped with a controller (Namil Optical Instruments, Ltd.) capable of adjusting the tensile strain and speed. All samples were uniaxially stretched up to 50% with a strain rate of 0.05 mm s^{-1}. The topography and conductive maps of Ag NW networks and composite electrodes were observed using an atomic force microscope (XE-100, Park's System) with conductive mode. The nanomechanical Young's modulus and their micromapping images of Ag NW networks and composite electrodes were obtained using the PinPoint Nano-mechanical mode of the Park's System atomic force microscope (NX 10). XPS surface analysis was performed by irradiating a 400 μm × 400 μm area of the sample using an Al-Kα X-ray source (1486.6 eV) (Nexsa, Thermo Fisher Scientific). XPS depth analysis was analyzed by sputtering a 1 mm × 1 mm area of samples by 1 cycle every 60 s using an Ar gas cluster with an ion energy of 8 keV as a sputtering source.

■ ASSOCIATED CONTENT

Supporting Information

The Supporting Information is available free of charge at https://pubs.acs.org/doi/10.1021/acsami.3c00965.

Performance of the PEDOT:PSS/EMIM:TCB electrode, B 1s, C 1s, Ag 3d XPS spectra; UPS spectra and work functions of the electrodes; device structures; mechanical and photovoltaic performances of reported Ag NW-based SOSCs (PDF)

■ AUTHOR INFORMATION

Corresponding Authors

Bumjoon J. Kim − *Department of Chemical and Biomolecular Engineering, Korea Advanced Institute of Science and Technology (KAIST), Daejeon 34141, Republic of Korea;* orcid.org/0000-0001-7783-9689; Email: bumjoonkim@kaist.ac.kr

Kookheon Char − *School of Chemical and Biological Engineering, Seoul National University, Seoul 08826, Republic of Korea;* orcid.org/0000-0002-7938-8022; Email: khchar@snu.ac.kr

Jeong Gon Son − *Soft Hybrid Materials Research Center, Korea Institute of Science and Technology, Seoul 02792, Republic of Korea; KU-KIST Graduate School of Converging Science and Technology, Korea University, Seoul 02841, Republic of Korea;* orcid.org/0000-0003-3473-446X; Email: jgson@kist.re.kr

Authors

Hyun Jeong Kwon − *Soft Hybrid Materials Research Center, Korea Institute of Science and Technology, Seoul 02792, Republic of Korea; School of Chemical and Biological Engineering, Seoul National University, Seoul 08826, Republic of Korea;* orcid.org/0000-0002-3834-5384

Geon-U Kim − *Department of Chemical and Biomolecular Engineering, Korea Advanced Institute of Science and Technology (KAIST), Daejeon 34141, Republic of Korea*

Chulhee Lim − *Department of Chemical and Biomolecular Engineering, Korea Advanced Institute of Science and Technology (KAIST), Daejeon 34141, Republic of Korea;* orcid.org/0000-0002-4904-7040

Jai Kyeong Kim − *Soft Hybrid Materials Research Center, Korea Institute of Science and Technology, Seoul 02792, Republic of Korea*

Sang-Soo Lee − *Soft Hybrid Materials Research Center, Korea Institute of Science and Technology, Seoul 02792, Republic of Korea;* orcid.org/0000-0001-5896-6471

Jinhan Cho − *Soft Hybrid Materials Research Center, Korea Institute of Science and Technology, Seoul 02792, Republic of Korea; Department of Chemical & Biological Engineering and KU-KIST Graduate School of Converging Science and Technology, Korea University, Seoul 02841, Republic of Korea;* orcid.org/0000-0002-7097-5968

Hyung-Jun Koo − *Department of Chemical & Biomolecular Engineering, Seoul National University of Science and Technology, Seoul 01811, Republic of Korea*

Complete contact information is available at: https://pubs.acs.org/10.1021/acsami.3c00965

Author Contributions

$^{\nabla}$H.J.K. and G-.UK. contributed equally to this work. The manuscript was written through the contributions of all

https://doi.org/10.1021/acsami.3c00965
ACS Appl. Mater. Interfaces 2023, 15, 13656−13667

authors. All authors have approved the final version of the manuscript.

Notes

The authors declare no competing financial interest.

■ ACKNOWLEDGMENTS

The authors gratefully acknowledge financial support from the Korea Institute of Science and Technology (KIST) Institutional Program (Project Nos. 2E32501 and 2E32503), KU-KIST program and the National Research Foundation of Korea (NRF) grant funded by the Korea government (MEST) (Nos. 2022R1A2B5B02001597, 2017M3D1A1039553, 2020M3D1A1110499, 2020M3D1A2101799, and 2020M3D1A2101800).

■ REFERENCES

(1) Shrivastava, S.; Trung, T. Q.; Lee, N.-E. Recent Progress, Challenges, and Prospects of Fully Integrated Mobile and Wearable Point-of-Care Testing Systems for Self-Testing. *Chem. Soc. Rev.* **2020**, *49*, 1812−1866.

(2) Nyein, H. Y. Y.; Bariya, M.; Tran, B.; Ahn, C. H.; Brown, B. J.; Ji, W.; Davis, N.; Javey, A. A Wearable Patch for Continuous Analysis of Thermoregulatory Sweat at Rest. *Nat. Commun.* **2021**, *12*, No. 1823.

(3) Lim, C.; Hong, Y. J.; Jung, J.; Shin, Y.; Sunwoo, S.-H.; Baik, S.; Park, O. K.; Choi, S. H.; Hyeon, T.; Kim, J. H.; Lee, S.; Kim, D.-H. Tissue-like Skin-Device Interface for Wearable Bioelectronics by Using Ultrasoft, Mass-Permeable, and Low-Impedance Hydrogels. *Sci. Adv.* **2021**, *7*, No. abd3716.

(4) Pu, Z.; Zhang, X.; Yu, H.; Tu, J.; Chen, H.; Liu, Y.; Su, X.; Wang, R.; Zhang, L.; Li, D. A Thermal Activated and Differential Self-Calibrated Flexible Epidermal Biomicrofluidic Device for Wearable Accurate Blood Glucose Monitoring. *Sci. Adv.* **2021**, *7*, No. abd0199.

(5) Son, D.; Kang, J.; Vardoulis, O.; Kim, Y.; Matsuhisa, N.; Oh, J. Y.; To, J. W.; Mun, J.; Katsumata, T.; Liu, Y.; McGuire, A. F.; Krason, M.; Molina-Lopez, F.; Ham, J.; Kraft, U.; Lee, Y.; Yun, Y.; Tok, J. B. H.; Bao, Z. An Integrated Self-Healable Electronic Skin System Fabricated via Dynamic Reconstruction of a Nanostructured Conducting Network. *Nat. Nanotechnol.* **2018**, *13*, 1057−1065.

(6) Cho, H.; Lee, B.; Jang, D.; Yoon, J.; Chung, S.; Hong, Y. Recent Progress in Strain-Engineered Elastic Platforms for Stretchable Thin-Film Devices. *Mater. Horiz.* **2022**, *9*, 2053−2075.

(7) Lim, M. S.; Nam, M.; Choi, S.; Jeon, Y.; Son, Y. H.; Lee, S. M.; Choi, K. C. Two-Dimensionally Stretchable Organic Light-Emitting Diode with Elastic Pillar Arrays for Stress Relief. *Nano Lett.* **2020**, *20*, 1526−1535.

(8) Koo, J. H.; Yun, H.; Lee, W.; Sunwoo, S.-H.; Shim, H. J.; Kim, D.-H. Recent Advances in Soft Electronic Materials for Intrinsically Stretchable Optoelectronic Systems. *Opto-Electron. Adv.* **2022**, *5*, 210131.

(9) Zhao, R.; Gu, Z.; Li, P.; Zhang, Y.; Song, Y. Flexible and Wearable Optoelectronic Devices Based on Perovskites. *Adv. Mater. Technol.* **2022**, *7*, No. 2101124.

(10) Ku, M.; Hwang, J. C.; Oh, B.; Park, J.-U. Smart Sensing Systems Using Wearable Optoelectronics. *Adv. Intell. Syst.* **2020**, *2*, No. 1900144.

(11) Wang, J.; Yan, C.; Chee, K. J.; Lee, P. S. Highly Stretchable and Self-Deformable Alternating Current Electroluminescent Devices. *Adv. Mater.* **2015**, *27*, 2876−2882.

(12) Li, D.; Lai, W.-Y.; Zhang, Y.-Z.; Huang, W. Printable Transparent Conductive Films for Flexible Electronics. *Adv. Mater.* **2018**, *30*, No. 1704738.

(13) Qiao, F.; Chu, H.; Xie, Y.; Weng, Z. Recent Progress of Transparent Conductive Electrodes in the Construction of Efficient Flexible Organic Solar Cells. *Int. J. Energy Res.* **2022**, *46*, 4071−4087.

(14) Fan, X. Doping and Design of Flexible Transparent Electrodes for High-Performance Flexible Organic Solar Cells: Recent Advances and Perspectives. *Adv. Funct. Mater.* **2021**, *31*, No. 2009399.

(15) Bagal, A.; Dandley, E. C.; Zhao, J.; Zhang, X. A.; Oldham, C. J.; Parsons, G. N.; Chang, C.-H. Multifunctional Nano-Accordion Structures for Stretchable Transparent Conductors. *Mater. Horiz.* **2015**, *2*, 486−494.

(16) McCoul, D.; Hu, W.; Gao, M.; Mehta, V.; Pei, Q. Recent Advances in Stretchable and Transparent Electronic Materials. *Adv. Electron. Mater.* **2016**, *2*, No. 1500407.

(17) Trung, T. Q.; Lee, N.-E. Materials and Devices for Transparent Stretchable Electronics. *J. Mater. Chem. C* **2017**, *5*, 2202−2222.

(18) Kim, K. S.; Zhao, Y.; Jang, H.; Lee, S. Y.; Kim, J. M.; Kim, K. S.; Ahn, J.-H.; Kim, P.; Choi, J.-Y.; Hong, B. H. Large-Scale Pattern Growth of Graphene Films for Stretchable Transparent Electrodes. *Nature* **2009**, *457*, 706−710.

(19) Bae, S.; Kim, H. R.; Lee, Y.; Xu, X.; Park, J.-S.; Zheng, Y.; Balakrishnan, J.; Lei, T.; Kim, H. R.; Song, Y., Il; Kim, Y.-J.; Kim, K. S.; Ozyilmaz, B.; Ahn, J.-H.; Hong, B. H.; Iijima, S. Roll-to-Roll Production of 30-Inch Graphene Films for Transparent Electrodes. *Nat. Nanotechnol.* **2010**, *5*, 574−578.

(20) Kraft, U.; Molina-Lopez, F.; Son, D.; Bao, Z.; Murmann, B. Ink Development and Printing of Conducting Polymers for Intrinsically Stretchable Interconnects and Circuits. *Adv. Electron. Mater.* **2020**, *6*, No. 1900681.

(21) Wang, Y.; Zhu, C.; Pfattner, R.; Yan, H.; Jin, L.; Chen, S.; Molina-Lopez, F.; Lissel, F.; Liu, J.; Rabiah, N. I.; Chen, Z.; Chung, J. W.; Linder, C.; Toney, M. F.; Murmann, B.; Bao, Z. A Highly Stretchable, Transparent, and Conductive Polymer. *Sci. Adv.* **2017**, *3*, No. e1602076.

(22) Dauzon, E.; Lin, Y.; Faber, H.; Yengel, E.; Sallenave, X.; Plesse, C.; Goubard, F.; Amassian, A.; Anthopoulos, T. D. Stretchable and Transparent Conductive PEDOT:PSS-Based Electrodes for Organic Photovoltaics and Strain Sensors Applications. *Adv. Funct. Mater.* **2020**, *30*, No. 2001251.

(23) Lipomi, D. J.; Vosgueritchian, M.; Tee, B. C. K.; Hellstrom, S. L.; Lee, J. A.; Fox, C. H.; Bao, Z. Skin-like Pressure and Strain Sensors Based on Transparent Elastic Films of Carbon Nanotubes. *Nat. Nanotechnol.* **2011**, *6*, 788−792.

(24) Lee, P.; Lee, J.; Lee, H.; Yeo, J.; Hong, S.; Nam, K. H.; Lee, D.; Lee, S. S.; Ko, S. H. Highly Stretchable and Highly Conductive Metal Electrode by Very Long Metal Nanowire Percolation Network. *Adv. Mater.* **2012**, *24*, 3326−3332.

(25) Ahn, S.; Choe, A.; Park, J.; Kim, H.; Son, J. G.; Lee, S.-S.; Park, M.; Ko, H. Directed Self-Assembly of Rhombic Carbon Nanotube Nanomesh Films for Transparent and Stretchable Electrodes. *J. Mater. Chem. C* **2015**, *3*, 2319−2325.

(26) Won, P.; Park, J. J.; Lee, T.; Ha, I.; Han, S.; Choi, M.; Lee, J.; Hong, S.; Cho, K. J.; Ko, S. H. Stretchable and Transparent Kirigami Conductor of Nanowire Percolation Network for Electronic Skin Applications. *Nano Lett.* **2019**, *19*, 6087−6096.

(27) Hong, S.; Lee, H.; Lee, J.; Kwon, J.; Han, S.; Suh, Y. D.; Cho, H.; Shin, J.; Yeo, J.; Ko, S. H. Highly Stretchable and Transparent Metal Nanowire Heater for Wearable Electronics Applications. *Adv. Mater.* **2015**, *27*, 4744−4751.

(28) Kang, S.; Cho, S.; Shanker, R.; Lee, H.; Park, J.; Um, D.-S.; Lee, Y.; Ko, H. Transparent and Conductive Nanomembranes with Orthogonal Silver Nanowire Arrays for Skin-Attachable Loudspeakers and Microphones. *Sci. Adv.* **2018**, *4*, No. eaas8772.

(29) Cho, S.; Kang, S.; Pandya, A.; Shanker, R.; Khan, Z.; Lee, Y.; Park, J.; Craig, S. L.; Ko, H. Large-Area Cross-Aligned Silver Nanowire Electrodes for Flexible, Transparent, and Force-Sensitive Mechanochromic Touch Screens. *ACS Nano* **2017**, *11*, 4346−4357.

(30) Kim, K. K.; Hong, S.; Cho, H. M.; Lee, J.; Suh, Y. D.; Ham, J.; Ko, S. H. Highly Sensitive and Stretchable Multidimensional Strain Sensor with Prestrained Anisotropic Metal Nanowire Percolation Networks. *Nano Lett.* **2015**, *15*, 5240−5247.

(31) Lee, J.; Lee, P.; Lee, H. B.; Hong, S.; Lee, I.; Yeo, J.; Lee, S. S.; Kim, T.-S.; Lee, D.; Ko, S. H. Room-Temperature Nanosoldering of a Very Long Metal Nanowire Network by Conducting-Polymer-Assisted Joining for a Flexible Touch-Panel Application. *Adv. Funct. Mater.* **2013**, *23*, 4171−4176.

https://doi.org/10.1021/acsami.3c00965
ACS Appl. Mater. Interfaces 2023, 15, 13656−13667

(32) Hsiao, S. T.; Tien, H. W.; Liao, W. H.; Wang, Y. S.; Li, S. M.; Mma, C. C.; Yu, Y. H.; Chuang, W. P. A Highly Electrically Conductive Graphene-Silver Nanowire Hybrid Nanomaterial for Transparent Conductive Films. *J. Mater. Chem. C* **2014**, *2*, 7284−7291.
(33) Shin, H.; Sharma, B. K.; Lee, S. W.; Lee, J.-B.; Choi, M.; Hu, L.; Park, C.; Choi, J. H.; Kim, T. W.; Ahn, J.-H. Stretchable Electroluminescent Display Enabled by Graphene-Based Hybrid Electrode. *ACS Appl. Mater. Interfaces* **2019**, *11*, 14222−14228.
(34) Pyo, J. B.; Kim, B. S.; Park, H.; Kim, T. A.; Koo, C. M.; Lee, J.; Son, J. G.; Lee, S.; Park, J. H. Floating Compression of Ag Nanowire Networks for Effective Strain Release of Stretchable Transparent Electrodes. *Nanoscale* **2015**, *7*, 16434−16441.
(35) Kim, B. S.; Shin, K.; Pyo, J. B.; Lee, J.; Son, J. G.; Lee, S.; Park, J. H. Reversibly Stretchable, Optically Transparent Radio-Frequency Antennas Based on Wavy Ag Nanowire Networks. *ACS Appl. Mater. Interfaces* **2016**, *8*, 2582−2590.
(36) Kim, B. S.; Pyo, J. B.; Son, J. G.; Zi, G.; Lee, S. S.; Park, J. H.; Lee, J. Biaxial Stretchability and Transparency of Ag Nanowire 2D Mass-Spring Networks Prepared by Floating Compression. *ACS Appl. Mater. Interfaces* **2017**, *9*, 10865−10873.
(37) Kim, B. S.; Kwon, H.; Kwon, H. J.; Pyo, J. B.; Oh, J.; Hong, S. Y.; Park, J. H.; Char, K.; Ha, J. S.; Son, J. G.; Lee, S. Buckling Instability Control of 1D Nanowire Networks for a Large-Area Stretchable and Transparent Electrode. *Adv. Funct. Mater.* **2020**, *30*, No. 1910214.
(38) Park, J. S.; Kim, G.; Lee, S.; Lee, J.; Li, S.; Lee, J.; Kim, B. J. Material Design and Device Fabrication Strategies for Stretchable Organic Solar Cells. *Adv. Mater.* **2022**, *34*, No. 2201623.
(39) Fan, X.; Nie, W.; Tsai, H.; Wang, N.; Huang, H.; Cheng, Y.; Wen, R.; Ma, L.; Yan, F.; Xia, Y. PEDOT:PSS for Flexible and Stretchable Electronics: Modifications, Strategies, and Applications. *Adv. Sci.* **2019**, *6*, No. 1900813.
(40) Badre, C.; Marquant, L.; Alsayed, A. M.; Hough, L. A. Highly Conductive Poly(3,4-Ethylenedioxythiophene):Poly (Styrenesulfonate) Films Using 1-Ethyl-3-Methylimidazolium Tetracyanoborate Ionic Liquid. *Adv. Funct. Mater.* **2012**, *22*, 2723−2727.
(41) Park, T.; Park, C.; Kim, B.; Shin, H.; Kim, E. Flexible PEDOT Electrodes with Large Thermoelectric Power Factors to Generate Electricity by the Touch of Fingertips. *Energy Environ. Sci.* **2013**, *6*, 788−792.
(42) Kim, S.; Lee, Y.; Lee, M.; An, S.; Cho, S.-J. Quantitative Visualization of the Nanomechanical Young's Modulus of Soft Materials by Atomic Force Microscopy. *Nanomaterials* **2021**, *11*, No. 1593.
(43) Garcia, R. Nanomechanical Mapping of Soft Materials with the Atomic Force Microscope: Methods, Theory and Applications. *Chem. Soc. Rev.* **2020**, *49*, 5850−5884.
(44) Teo, M. Y.; Kim, N.; Kee, S.; Kim, B. S.; Kim, G.; Hong, S.; Jung, S.; Lee, K. Highly Stretchable and Highly Conductive PEDOT:PSS/Ionic Liquid Composite Transparent Electrodes for Solution-Processed Stretchable Electronics. *ACS Appl. Mater. Interfaces* **2017**, *9*, 819−826.
(45) Park, H.; Lee, J. H.; Lee, S.; Jeong, S. Y.; Choi, J. W.; Lee, C. L.; Kim, J. H.; Lee, K. Retarding Ion Exchange between Conducting Polymers and Ionic Liquids for Printable Top Electrodes in Semitransparent Organic Solar Cells. *ACS Appl. Mater. Interfaces* **2020**, *12*, 2276−2284.
(46) Jeong, S. H.; Woo, S. H.; Han, T. H.; Park, M. H.; Cho, H.; Kim, Y. H.; Cho, H.; Kim, H.; Yoo, S.; Lee, T. W. Universal High Work Function Flexible Anode for Simplified Ito-Free Organic and Perovskite Light-Emitting Diodes with Ultra-High Efficiency. *NPG Asia Mater.* **2017**, *9*, No. e411.
(47) Lee, J.; Lim, C.; Lee, S.; Jeon, Y.; Lee, S.; Kim, T.; Lee, J.; Kim, B. J. Intrinsically Stretchable and Non-Halogenated Solvent Processed Polymer Solar Cells Enabled by Hydrophilic Spacer-Incorporated Polymers. *Adv. Energy Mater.* **2022**, *12*, No. 2202224.
(48) Lee, J.; Kim, G.; Kim, D. J.; Jeon, Y.; Li, S.; Kim, T.; Lee, J.; Kim, B. J. Intrinsically-Stretchable, Efficient Organic Solar Cells Achieved by High-Molecular-Weight, Electro-Active Polymer Acceptor Additives. *Adv. Energy Mater.* **2022**, *12*, No. 2200887.
(49) Wang, Z.; Xu, M.; Li, Z.; Gao, Y.; Yang, L.; Zhang, D.; Shao, M. Intrinsically Stretchable Organic Solar Cells beyond 10% Power Conversion Efficiency Enabled by Transfer Printing Method. *Adv. Funct. Mater.* **2021**, *31*, No. 2103534.
(50) Savagatrup, S.; Makaram, A. S.; Burke, D. J.; Lipomi, D. J. Mechanical Properties of Conjugated Polymers and Polymer-Fullerene Composites as a Function of Molecular Structure. *Adv. Funct. Mater.* **2014**, *24*, 1169−1181.
(51) Sawyer, E. J.; Zaretski, A. V.; Printz, A. D.; de los Santos, N. V.; Bautista-Gutierrez, A.; Lipomi, D. J. Large Increase in Stretchability of Organic Electronic Materials by Encapsulation. *Extreme Mech. Lett.* **2016**, *8*, 78−87.
(52) Li, L.; Liang, J.; Gao, H.; Li, Y.; Niu, X.; Zhu, X.; Xiong, Y.; Pei, Q. A Solid-State Intrinsically Stretchable Polymer Solar Cell. *ACS Appl. Mater. Interfaces* **2017**, *9*, 40523−40532.
(53) Zhu, Q.; Xue, J.; Zhang, L.; Wen, J.; Lin, B.; Naveed, H. B.; Bi, Z.; Xin, J.; Zhao, H.; Zhao, C.; Zhou, K.; Liu, S. F.; Ma, W. Intermolecular Interaction Control Enables Co-optimization of Efficiency, Deformability, Mechanical and Thermal Stability of Stretchable Organic Solar Cells. *Small* **2021**, *17*, No. 2007011.
(54) Cheng, Y. J.; Yang, S. H.; Hsu, C. S. Synthesis of Conjugated Polymers for Organic Solar Cell Applications. *Chem. Rev.* **2009**, *109*, 5868−5923.
(55) Fukuda, K.; Yu, K.; Someya, T. The Future of Flexible Organic Solar Cells. *Adv. Energy Mater.* **2020**, *10*, No. 2000765.
(56) Zhang, J.; Tan, H. S.; Guo, X.; Facchetti, A.; Yan, H. Material Insights and Challenges for Non-Fullerene Organic Solar Cells Based on Small Molecular Acceptors. *Nat. Energy* **2018**, *3*, 720−731.
(57) Lee, J.-W.; Sun, C.; Lee, S.-W.; Kim, G.-U.; Li, S.; Wang, C.; Kim, T.-S.; Kim, Y.-H.; Kim, B. J. Sequentially Regular Polymer Acceptors Featuring Flexible Spacers for High-Performance and Mechanically Robust All-Polymer Solar Cells. *Energy Environ. Sci.* **2022**, *15*, 4672−4685.
(58) Lee, J. W.; Jeong, D.; Kim, D. J.; Phan, T. N. L.; Park, J. S.; Kim, T. S.; Kim, B. J. Flexible-Spacer Incorporated Polymer Donors Enable Superior Blend Miscibility for High-Performance and Mechanically-Robust Polymer Solar Cells. *Energy Environ. Sci.* **2021**, *14*, 4067−4076.
(59) Noh, J.; Kim, G.-U.; Han, S.; Oh, S. J.; Jeon, Y.; Jeong, D.; Kim, S. W.; Kim, T.-S.; Kim, B. J.; Lee, J.-Y. Intrinsically Stretchable Organic Solar Cells with Efficiencies of over 11%. *ACS Energy Lett.* **2021**, *6*, 2512−2518.
(60) Wu, Z.; Sun, C.; Dong, S.; Jiang, X. F.; Wu, S.; Wu, H.; Yip, H. L.; Huang, F.; Cao, Y. N-Type Water/Alcohol-Soluble Naphthalene Diimide-Based Conjugated Polymers for High-Performance Polymer Solar Cells. *J. Am. Chem. Soc.* **2016**, *138*, 2004−2013.
(61) Wang, M.; Sun, J.; Cai, X.; Huang, Y.; Li, F. Morphology Modulation of Organic Photovoltaics with Block Copolymer Additive Based on Rational Design Strategies. *Org. Electron.* **2021**, *88*, No. 106020.

https://doi.org/10.1021/acsami.3c00965
ACS Appl. Mater. Interfaces 2023, 15, 13656−13667